Eigenmodes for metal-dielectric light-transmitting nanostructures

B. Sturman and E. Podivilov

Institute of Automation and Electrometry, 630090 Novosibirsk, Russia

M. Gorkunov

Institute of Crystallography, Russian Academy of Sciences, Leninskii pr. 59, 117333 Moscow, Russia
and Department of Mathematics, University of Strathclyde, 26 Richmond Street, Glasgow G1 1XH, United Kingdom

We show that the concept of optical eigenmodes in lossless waveguide structures, which assumes the separation into propagating and evanescent modes, fails in the case of metal-dielectric structures. In addition to these modes, there is a sequence of new eigenstates with complex values of the propagation constant and nonvanishing lateral energy flows. The whole eigenmode problem ceases to be Hermitian because of changing sign of the optical dielectric constant. Particular examples of the waveguide structures include single slits, one-dimensional photonic crystals, and circular holes. The emphasis is made on the structures with nanoholes (whose sizes are considerably smaller than the light wavelength) possessing propagation modes and showing an extraordinary high light transmission. The results obtained form a necessary basis for modelling of this phenomenon.

PACS number(s): 42.25.Bs, 42.25.Fx, 42.70.Qs, 73.20.Mf

I. INTRODUCTION

The concept of eigenmodes lies at the center of any physical problem for optical light-transmitting systems including waveguides and photonic crystals. This concept seems to be complete and the general properties of the eigenvalues and eigenfunctions seem to be fully presented in numerous textbooks and reviews.[1–8]

For photonic crystals (PCs), determination of the band structures—the eigenfrequencies and eigenfunctions versus the quasi-wave-vector—is the most common. The eigenfrequencies are proven to be real for any lossless PC, i.e., for any periodic spatial distribution of real dielectric optical permittivity $\varepsilon(\mathbf{r})$. A close analogy with the electronic band states is well established.[6,7]

An alternative formulation of the eigenmode problem is typical of waveguide systems, single slits and holes, one-dimensional (1D) and two-dimensional (2D) PCs, etc., which are uniform along the propagation coordinate z. Here one must find all allowed values of the propagation constant β entering the propagation factor $\exp(i\beta z)$ and the corresponding transverse (in x and y) distributions of the optical light fields. This formulation is important not only for description of the propagating properties of the medium but also for calculations of the transmission-reflection coefficients at different interfaces and/or junctions. Completeness of the set of the eigenfunctions is crucial in the second case.

Among the waveguiding systems, most efforts have been spent to investigate dielectric waveguides and dielectric PCs.[1–4] It is proven for the lossless dielectric systems ($\varepsilon > 0$) that the admitted values of β^2 are always real—positive and negative. The corresponding eigenmodes are propagating and evanescent, respectively, and a close analogy with quantum mechanics holds true. The same is valid for the ideal-metal waveguiding systems, $\varepsilon \to \infty$.[9,10]

The situation with metal-dielectric systems is different. A part of general sources, see, e.g., Refs. 3, 4, and 10, avoid the case of real metals. Quite often, e.g., Refs. 1 and 5, the authors refer to an analogy with the dielectric case. Some sources, see, e.g., Refs. 8 and 11, are dealing with engineering calculations of metal-clad waveguides without considerations of their general properties. The general point of view is that the separation on the propagating and evanescent modes and the analogy with quantum mechanics holds true for lossless metals and β^2 becomes complex only in the presence of dissipative losses ($\varepsilon'' = \mathrm{Im}\,\varepsilon \neq 0$).[1] At the same time, one can find a soft general warning (without clarifications) that the above point of view can be not quite correct.[2] Among the literature, we know a couple of papers[12,13] where the authors mention, on the basis of particular model calculations, that some values of β^2 cease to be real for $\varepsilon'' = 0$. It seems to be that the above warnings remain unknown and/or not understood in the optical community.

A permanently growing interest to metal-based systems is usually attributed to the excitation of the surface plasmons which allow the light confinement on the subwavelength (nano) scale.[1,14,15] The necessary conditions, $\varepsilon' = \mathrm{Re}\,\varepsilon < -1$, $\varepsilon'' = \mathrm{Im}\,\varepsilon \ll |\varepsilon'|$, are fulfilled for many metals. For example, for silver at the wavelength $\lambda \simeq 500$ nm we have $\varepsilon' \simeq -9.6$ and $\varepsilon'' \simeq 0.3$.[16] The limit of lossless metal ($\varepsilon' < 0$, $\varepsilon'' = 0$) is as actual as that of lossless dielectric.

Discovery of the extraordinarily light transmission (ELT) through subwavelength holes and slits in metal films in 1998[15,17] has strongly enhanced the interest to metal-based nanostructures. Plenty of experimental and theoretical studies on the ELT have been performed since then, see, e.g., Refs. 18–22 and references therein. However, the main mechanisms and parametric dependences of this fundamental phenomenon remain still not well understood; descriptions of the ELT heavily rely on numerical simulations and/or over-simplified models.

Setting aside details, outcomes, and problems of the ELT theory, we mention only that the accepted calculation schemes (except for direct numerical methods) imply the
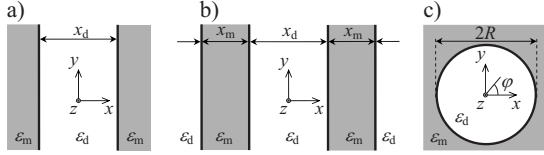
FIG. 1. Three waveguiding structures, a single slit (a), a periodic 1D structure (b), and a circular hole (c). The permittivities of dielectric and metal are ε_d and ε_m, respectively.

knowledge of the eigenmodes.[13,23] The present notion of eigenmodes for metal-dielectric waveguide structures (1D and 2D PCs, arrays of holes and single holes in metals, etc.) is insufficient not only because of the above-mentioned general gap. Historically, the studies of metal-based waveguides were focused mostly on slits and holes whose size is comparable with or larger than the light wavelength. Surprisingly little is known about the properties of the eigenmodes, including those of the propagating modes, in the opposite case of subwavelength slits and/or holes.[18]

The purposes of this paper are the following:

(i) To show that the generally accepted concept of eigenmodes is insufficient for the case of lossless metal-dielectric waveguide structures.

(ii) To establish the general properties of new (anomalous) eigenmodes which are neither propagating nor evanescent.

(iii) To characterize the propagating modes in the subwavelength domain, including the case of slits and holes whose sizes are much smaller than the light wavelength.

The text is structured as follows: In Sec. II, we explain in general terms why the analogy with quantum mechanics, which holds in the dielectric case, fails for metal-dielectric structures. In the subsequent Secs. III–V we analyze three basic structures. They are a single dielectric slit of thickness x_d in a metal, Fig. 1(a); a 1D metal-dielectric PC consisting of an alternating sequence of layers with permittivities $\varepsilon_{d,m}$ and thicknesses $x_{d,m}$, Fig. 1(b); and a circular hole of radius R in a metal, Fig. 1(c). Conclusions are drawn in Sec. VI.

II. WHY THE ANALOGY WITH QUANTUM MECHANICS FAILS

To catch the specifics of the eigenmode problem in the metal-dielectric case, we consider a 1D photonic crystal assuming that the permittivity ε is a real periodic function of the coordinate x. No more restrictions are imposed yet. The electric and magnetic light-field amplitudes, $\mathbf{E}=(E_x,E_y,E_z)$ and $\mathbf{H}=(H_x,H_y,H_z)$, are superpositions of independent TE and TM modes in the 1D case.[9,10] New results in this case refer only to the TM modes. The only nonzero component of the magnetic field for such modes is $H=H_y$. It is representable as $H=h(x)\exp(i\beta z)$. Maxwell's equations give for the eigenfunction $h=h(x)$ the following well known equation:

$$\hat{L}h=\beta^2 h, \quad \hat{L}=\varepsilon\frac{d}{dx}\frac{1}{\varepsilon}\frac{d}{dx}+\varepsilon k_0^2, \tag{1}$$

where $k_0=2\pi/\lambda$ and λ is the vacuum wavelength. This sets an eigenmode problem for the differential operator $\hat{L}$ with β^2

being the eigenvalue. The values $\beta=\pm\sqrt{\beta^2}$ correspond to the propagation in the $\pm z$ directions. The nonzero components of the light electric field, E_x and E_z, are expressed by H from Maxwell's equations, $E_x=\beta H/\varepsilon k_0$, $E_z=(i/\varepsilon k_0)\partial H/\partial x$.

The conclusion about reality of the eigenvalue β^2 and about analogy with quantum mechanics is generally based on the Hermitian character of the operator $\hat{L}$, i.e., on the property

$$\langle h_2|\hat{L}h_1\rangle=\langle h_1|\hat{L}h_2\rangle^*, \tag{2}$$

where $\langle\cdots|\cdots\rangle$ stands for the scalar product and the asterisk means complex conjugation. The scalar product of two complex functions $h_1(x)$ and $h_2(x)$, denoted as $\langle h_2|h_1\rangle$, must meet certain mathematical requirements (axioms).[24] One can make sure using Eq. (1) that the most common (but not general) definition of the scalar product,

$$\langle h_2|h_1\rangle=\int h_2^*(x)h_1(x)dx, \tag{3}$$

is not compatible with Eq. (2). To satisfy this equation, one can redefine the scalar product as

$$\langle h_2|h_1\rangle_\varepsilon=\int \varepsilon^{-1}(x)h_2^*(x)h_1(x)dx, \tag{4}$$

the subscript ε indicates the use of the weight function $\varepsilon^{-1}(x)$. In the dielectric case, $\varepsilon(x)>0$, this definition meets all axioms of the scalar product,[24] which proves reality of β^2. However, in the metal-dielectric case, where $\varepsilon(x)$ is a sign-changing function, it contradicts to one of the axioms—the norm squared $\langle h|h\rangle_\varepsilon$ ceases to be positively defined. Therefore, the conclusions about Hermitian character of $\hat{L}$ and about reality of β^2 cannot be made in this case.[25]

It is useful to supplement the general considerations by a simple remark. The direct check of the Hermitian property for PCs includes an integration by parts and implies vanishing contributions at $\pm\infty$. The standard way to deal with this situation is to impose the cycling boundary conditions for an arbitrary large number of elementary cells and to then turn this number to infinity.[26] The use of the Fourier transformation and manipulation with infinite-rank matrices to treat the general properties of the eigenmodes, which happens often in the literature, seems to be much less effective.

With the basic difference from the dielectric case explained, we can proceed to useful assertions using the definition of the scalar product given by Eq. (4).

If an eigenfunction $h(x)$ possesses a positive norm, the corresponding value of β^2 is real. Within the subspace of such functions, all the axioms of the scalar product are fulfilled.

Two eigenfunctions h_1 and h_2 corresponding to different real eigenvalues β_1^2 and β_2^2 are orthogonal, $\langle h_2|h_1\rangle_\varepsilon=0$. This can be proven by multiplying Eq. (1) for $h_{1,2}$ by $h_{2,1}^*$, integrating by parts, and using the boundary conditions at the metal-dielectric interfaces.

If at least one of $\beta_{1,2}^2$ is complex, this orthogonality relation must be replaced by $\langle h_2^*|h_1\rangle_\varepsilon=\int\varepsilon^{-1}h_2h_1dx=0$.
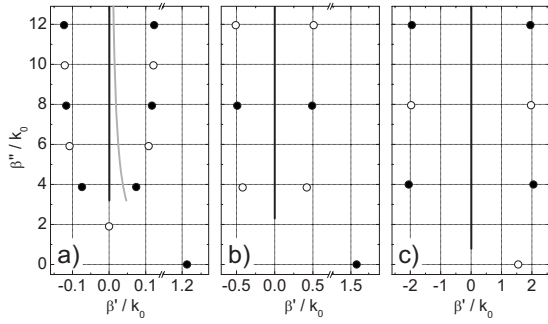
FIG. 2. The values of the propagation constant β for a single slit of the width x_d for $\varepsilon_d=1$ and three combinations of parameters ε_m and x_d/λ: (a) $\varepsilon_m=-10$, $x_d/\lambda=1/4$; (b) $\varepsilon_m=-5$, $x_d/\lambda=1/8$; (c) $\varepsilon_m=-0.64$, $x_d/\lambda=1/8$. The filled and open circles refer to the even and odd modes, respectively. The vertical black lines show the continuous spectrum. The gray line in case (a) shows the continuous spectrum with weak losses ($\varepsilon_m''=0.3$ as in silver) taken into account. Note the breaks in the horizontal axis in cases (a) and (b).

The above general properties occur also in the case of a single slit in a lossless metal. The use of the cycling boundary conditions is not necessary here because the eigenmodes with complex eigenvalues are fully localized; the corresponding eigenfunctions are zero at infinity.

In the 2D case, the Hermitian character of the eigenmode problem and reality of β^2 can be proven only in the case of waves with $E_z=0$ (TE modes). In the general case (TM and hybrid modes) complex values of β^2, i.e., the anomalous modes, are present.

The question arises whether the above features of the metal-dielectric structures lead to complex eigenfrequency ω for photonic crystals. The answer is no: The eigenfrequencies are real in the lossless case. The reason is as follows: To formulate the eigenproblem for the frequency, we must replace k_0 by ω/c (c is the speed of light) in Eq. (1) and to divide its left- and right-hand sides by ε. The corresponding differential operator for the eigenvalue ω^2 becomes Hermitian if we use the definition (3) for the scalar product. In other words, our proof of the non-Hermitian character of the eigenproblem for β^2 is fully compatible with the general proof of reality of the eigenfrequency ω in photonic crystals which is given in Ref. 6.

III. SINGLE SLIT

This waveguiding structure is presented in Fig. 1(a). Within the slit, $|x|<x_d/2$, we have a dielectric with the permittivity $\varepsilon=\varepsilon_d$ and outside the slit, $|x|>x_d/2$, we have a metal with the permittivity $\varepsilon=\varepsilon_m$; the quantities $\varepsilon_{d,m}$ are generally complex.

The main findings for this structure can be announced with the help of Fig. 2 which shows the allowed values of the propagation constant $\beta=+\sqrt{\beta^2}$ in the lossless case for three representative sets of parameters. We always have a sequence of anomalous complex values, $\beta=\beta'+i\beta''$ with $\beta''>\sqrt{|\varepsilon_m|}$ and $\beta'=\pm|\beta'|$, which originates from the complex conjugate eigenvalues β^2, and a continuous spectrum $\beta'=0$, $\beta''>\sqrt{|\varepsilon_m|}$. Furthermore, we have at least one propagation

mode with $\beta'>0$ and $\beta''=0$. If the slit width x_d is not too small, we also have discrete evanescent mode (modes) with $\beta'=0$ and $\beta''>0$. Below in this section we present the properties of these eigenmodes in more detail.

According to Eq. (1) the eigenfunction h obeys the equation

$$d^2h/dx^2 + (\varepsilon k_0^2 - \beta^2)h = 0 \qquad (5)$$

within the metal and dielectric regions. Its particular solutions in these regions are exponential functions $\exp(\pm ip_d x)$ and $\exp(\pm ip_m x)$, where

$$p_{d,m} = \sqrt{\varepsilon_{d,m}k_0^2 - \beta^2}. \qquad (6)$$

The square root of a complex number w is defined according to the complex variable theory: $0<\arg(\sqrt{w})\leqslant\pi/2$ for $w''\geqslant 0$ and $-\pi/2<\arg(\sqrt{w})<0$ for $w''<0$.

A. Discrete spectrum: Localized solutions

Within the slit region, $|x|<x_d/2$, the general solution for $h(x)$ is

$$h = c_+e^{ip_d x} + c_-e^{-ip_d x} \qquad (7)$$

with two constants $c_\pm$. Outside the slit we can represent $h(x)$ as

$$h = b_+e^{ip_m x} \quad (x>x_d/2),$$

$$h = b_-e^{-ip_m x} \quad (x<-x_d/2), \qquad (8)$$

where $b_\pm$ are new constants. If $p_m''>0$, then $h(x)\to 0$ for $|x|\to\infty$, i.e., we have a localized solution.

Using the boundary conditions (continuity of H and $E_z \propto \varepsilon^{-1}\partial H/\partial x$ as functions of x) one can readily come to a set of four linear equations for constants $c_\pm$ and $b_\pm$. From the condition of solvability of this set (the zero-determinant condition) we obtain routinely the following dispersion equation for β^2:

$$e^{ip_d x_d} = \pm\frac{p_d\varepsilon_m + p_m\varepsilon_d}{p_d\varepsilon_m - p_m\varepsilon_d}. \qquad (9)$$

Alternatively, we can represent the eigenfunction $h(x)$ outside the slit as

$$h = b_+e^{-ip_m x} \quad (x>x_d/2),$$

$$h = b_-e^{ip_m x} \quad (x<-x_d/2). \qquad (10)$$

The only difference with Eqs. (8) is the signs before p_m. The function $h(x)$ decreases for $|x|\to\infty$ when $p_m''<0$. The dispersion equation for this case reads

$$e^{-ip_d x_d} = \pm\frac{p_d\varepsilon_m + p_m\varepsilon_d}{p_d\varepsilon_m - p_m\varepsilon_d}. \qquad (11)$$

It can be obtained from Eq. (9) by the replacement $p_m \to -p_m$. As we will see below, Eqs. (9) and (11) supplement each other in different regions of β^2.

Combining the linear algebraic relations for the coefficients $c_\pm$ and $b_\pm$, one can prove easily that signs $(+)$ and $(-)$

on the right-hand sides of the dispersion equations correspond to the even, $h(x) = h(-x)$, and odd, $h(x) = -h(-x)$, eigenmodes, respectively.

In the general case, the normalized propagation constant β/k_0 is determined by three dimensionless parameters, $k_0 x_d$, ε_m, and ε_d. It is sufficient, however, to investigate the dependence of β only on the first two parameters by setting $\varepsilon_d = 1$ (an air slit). Then we can calculate β for $\varepsilon_d \neq 1$ using the scaling relation

$$\beta(k_0 x_d, \varepsilon_m, \varepsilon_d) = \sqrt{\varepsilon_d}\,\beta(\sqrt{\varepsilon_d}\,k_0 x_d, \varepsilon_m/\varepsilon_d, 1), \qquad (12)$$

which complies with the above dispersion equations. As follows from this relation, it is possible to shape the properties of the slit (the relative permittivity of the metal $\varepsilon_m/\varepsilon_d$ and the effective width $\sqrt{\varepsilon_d}\,x_d$) by filling the slit with a dielectric with $\varepsilon_d \neq 1$. Apparently, transparent dielectrics with large refractive index $\sqrt{\varepsilon_d}$, which considerably increases the effective slit width, are most suitable for this purpose.

1. Propagating and evanescent modes

Consider first *real* eigenvalues (positive and negative) for $\beta^2/k_0^2 > -|\varepsilon_m'|$ and $\varepsilon_m'' = 0$. In this range we have $p_m'' > 0$ so that Eq. (9) must be used to analyze the localized modes.

In the subrange $\beta^2/k_0^2 > 1$, where $p_{d,m}$ are pure imaginary, Eq. (9) can be rewritten as $k_0 x_d = F_\pm(\xi, |\varepsilon_m|)$, where $\xi = \beta^2/k_0^2$ and

$$F_\pm = \frac{1}{\sqrt{\xi - 1}} \ln\left(\pm \frac{|\varepsilon_m|\sqrt{\xi - 1} + \sqrt{\xi + |\varepsilon_m|}}{|\varepsilon_m|\sqrt{\xi - 1} - \sqrt{\xi + |\varepsilon_m|}} \right). \qquad (13)$$

It gives solutions for ξ as a function of $|\varepsilon_m|$ and $k_0 x_d$. If $|\varepsilon_m| > 1$ (the most common case), the function $F_-(\xi)$ grows from $2|\varepsilon_m|/\sqrt{|\varepsilon_m| + 1}$ to ∞ when ξ increases from 1 to $\xi_c = |\varepsilon_m|/(|\varepsilon_m| - 1)$; for $\xi > \xi_c$ the function $F_-(\xi)$ is not defined. On the contrary, the function $F_+(\xi)$ is defined only for $\xi > \xi_c$; it decreases here monotonically from ∞ to 0 with increasing argument. As follows from these observations, for any finite values of $k_0 x_d$ and $|\varepsilon_m|$ there is one solution of Eq. (13) for $\xi \equiv \beta^2/k_0^2$ which corresponds to the even propagating mode, i.e., to sign (+) in Eq. (13). The root ξ that refers to the odd propagating mode (−), exists only for $k_0 x_d > 2|\varepsilon_m|/\sqrt{|\varepsilon_m| + 1}$, i.e., for sufficiently large slit widths. The biggest value of β^2/k_0^2 always corresponds to the even propagating mode. Line 1 and the section of line 2 with $\xi > 1$ in Fig. 3(a) show the functions $F_+(\xi)$ and $F_-(\xi)$, respectively, for $\varepsilon_m = -5$.

In the subrange $-|\varepsilon_m| < \xi < 1$ parameter p_d becomes real while p_m remains imaginary. Equation (9) with sign (+) (even modes) can be rewritten here as $k_0 x_d = F_+(\xi, |\varepsilon_m|)$, where

$$F_+ = \frac{2\pi n}{\sqrt{1 - \xi}} - \frac{2}{\sqrt{1 - \xi}} \arctan\left(\frac{\sqrt{|\varepsilon_m| + \xi}}{|\varepsilon_m|\sqrt{1 - \xi}} \right) \qquad (14)$$

and $n = 1, 2, \dots$ To obtain the function $F_-(\xi, |\varepsilon_m|)$ for the odd modes, it is sufficient to replace $2n$ by $2n - 1$.

The found relations give a sequence of branches for $k_0 x_d$ as a function of $\xi \equiv \beta^2/k_0^2$. The structure of the lowest branches for $|\varepsilon_m| > 1$ is shown in Fig. 3(a) by lines 2–4. The
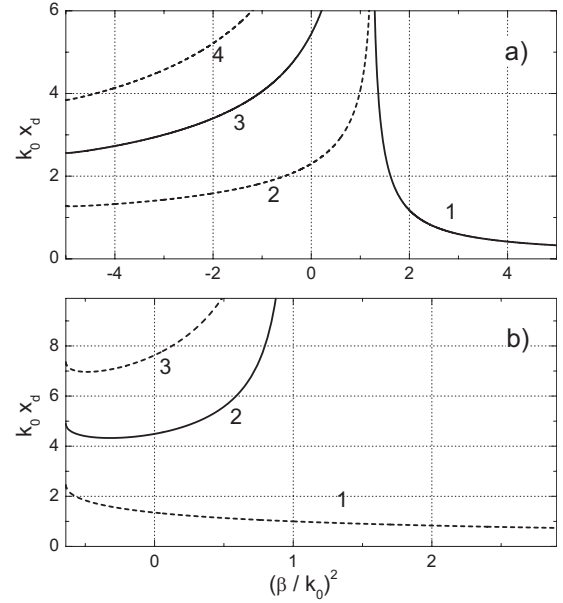
FIG. 3. Dependence of $k_0 x_d$ on $\xi \equiv \beta^2/k_0^2$ for the propagating ($\xi > 0$) and evanescent ($-|\varepsilon_m| < \xi < 0$) modes; (a) and (b) correspond to $\varepsilon_m = -5$ and -0.64. The solid and dashed lines refer to the even and odd modes. Note that branches 1,2 and 3,4 in case (a) turn to infinity at $\xi = 5/4$ and 1, respectively.

lowest branch 2 corresponds to the odd mode with $n = 1$, it transforms to the odd branch of the previous range, $\xi > 1$. The other branches are finite at the left end ($\xi = -|\varepsilon_m|$) and turn to infinity at the right end ($\xi = 1$). The larger the number n, the higher is the branch. Note that each branch possesses a shallow minimum in the close vicinity of the left end. In particular, the minimum of branch 2 in Fig. 3(a) occurs at $\beta^2/k_0^2 \approx 4.9$. The minima become more pronounced with decreasing $|\varepsilon_m|$.

As follows from these observations, within the interval $-|\varepsilon_m| < \xi < 1$ the number of propagating and evanescent modes increases with increasing $k_0 x_d$ and new even or odd modes appear in pairs. With decreasing $k_0 x_d$, all these modes disappear sooner or later depending on $|\varepsilon_m|$. The odd evanescent mode with $n = 1$ disappears last. For the threshold value of $k_0 x_d$ we have $(k_0 x_d)_{th} \approx \pi/\sqrt{|\varepsilon_m| + 1}$; it decreases with increasing $|\varepsilon_m|$.

In the case $|\varepsilon_m| < 1$, which can be realized, e.g., with aluminum[28] or employing the relative permittivity $\varepsilon_m/\varepsilon_d$, the structure of branches is different. In the subrange $\xi > 1$, the only solution of equation $k_0 x_d = F_\pm(\xi)$ corresponds to sign (−), i.e., to the odd propagating mode. This branch continues without any singularity into the region $-|\varepsilon_m| < \xi < 1$, where it corresponds to the lowest of the odd branches, see Fig. 3(b). In the whole range of $\xi \equiv \beta^2/k_0^2$ the lowest branch of $F_-(\xi)$ is decreasing. The structure of the higher branches of $F_\pm(\xi)$ is qualitatively the same as it is in the case $|\varepsilon_m| > 1$; the main quantitative difference is the more pronounced minima near the left end.

In any case, only a single propagating mode with $\beta/k_0 > 1$ survives for sufficiently small slit width parameter $k_0 x_d$. We consider now this important mode in some detail for $|\varepsilon_m| > 1$ taking into account small losses ($\varepsilon_m'' \neq 0$). For $k_0 x_d \ll 1$, we obtain from Eq. (9),

$$\beta \simeq \frac{1}{x_d}\left[\ln\left(\frac{|\varepsilon_m'|+1}{|\varepsilon_m'|-1}\right)+\frac{2i\varepsilon_m''}{|\varepsilon_2'|^2-1}\right]. \qquad (15)$$

The effective refractive index β'/k_0 tends to infinity for $x_d \to 0$ while the ratio β'/β'', i.e., the quality factor of the mode, remains constant. In the ideal-metal limit ($|\varepsilon_m|\to\infty$) we have $\beta/k_0=0$.

Note that in the opposite case, $x_d\to\infty$, we have the following from Eq. (9): $\beta'/k_0=\pm\sqrt{|\varepsilon_m'|/(|\varepsilon_m'|-1)}$. This corresponds to the usual surface plasmon which exists under the condition $\varepsilon_m'<-1$.[1,9]

2. Anomalous eigenvalues

Above we restricted ourselves to the real values of $\xi = \beta^2/k_0^2$. However, the localized eigenmodes possess also complex eigenvalues in the lossless case, $\varepsilon_m''=0$. To find them, we must use both Eqs. (9) and (11). Numerical analysis of Eq. (9) gives a sequence of complex roots for ξ; for all of them we have $p_m''>0$, i.e., the localized modes. Equation (11) gives the complex conjugate sequence of roots. For all of them $p_m''<0$, which also satisfies the condition of localization, $h(\pm\infty)=0$. In the dielectric case, $\varepsilon_m>0$, the complex eigenvalues are absent.

Figure 2 shows the anomalous values of β/k_0 for three representative combinations of parameters ε_m and k_0x_d. Numerical and analytical studies have allowed us to establish some general properties of the anomalous eigenvalues:

(i) For the anomalous roots we have generally $\beta''/k_0 > \sqrt{|\varepsilon_m|}$.

(ii) For subwavelength slits $\beta''\simeq n\pi/x_d$ and $p_dx_d\simeq n\pi$ with $n=1,2,\ldots$. The anomalous modes can be attributed thus to the transverse cavity resonances.

(iii) The vertical separation between the anomalous roots of the same parity (even or odd) is $\simeq 2\pi/x_d$.

(iv) The horizontal separation between the anomalous roots, $2|\beta'|$, is relatively small, $|\beta'|<|\beta''|$; it is decreasing with increasing $|\varepsilon_m|$ and/or k_0x_d.

(v) With increasing β'', the horizontal separation is slowly increasing for $|\varepsilon_m|>1$ and decreasing for $|\varepsilon_m|<1$.

With changing parameters k_0x_d and $|\varepsilon_m|$, pairs of anomalous roots transform into pairs of evanescent roots of the same symmetry (even or odd) and vice versa. Such transformations occur in the vicinity of $\beta/k_0=i\sqrt{|\varepsilon_m|}$; they are closely related to the mentioned shallow minima of $F_\pm(\xi)$.

A representative example of such transformations is given by Fig. 4 for $\varepsilon_m=-10$. Let us decrease the slit width parameter k_0x_d starting from 0.95. For this value only a single evanescent root with $\beta/k_0\simeq 3.115i$ is present. With decreasing slit width, new evanescent root with $\beta/k_0=i\sqrt{10}\simeq 3.162i$ splits off from the continuous spectrum at $k_0x_d=\pi/\sqrt{|\varepsilon_m|+1}\simeq 0.9472$. Two imaginary roots then move towards each other to confluence at $(k_0x_d)_{th}\simeq 0.9453$. For $k_0x_d<(k_0x_d)_{th}$ we have a pair of anomalous roots. The horizontal separation between them, $2|\beta'/k_0|$, increases sharply with departure from the threshold while β''/k_0 grows almost linearly with decreasing slit width.

The same scenario of generation of the anomalous roots takes place each time when an evanescent root approaches
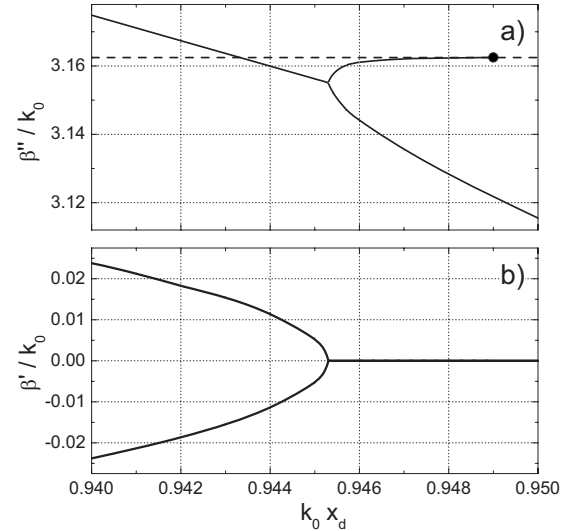
FIG. 4. Transformation between pairs of evanescent and anomalous roots near the border of the continuous spectrum (shown by the horizontal dashed line) when changing the slit width parameter k_0x_d for $\varepsilon_m=-10$. The dot marks separation of the discrete evanescent root from the continuous spectrum.

the border of the continuous spectrum, $\beta/k_0=i\sqrt{|\varepsilon_m|}$. With increasing slit width, pairs of the anomalous roots transform sequentially into the evanescent roots.

3. Eigenfunctions

As we know, the eigenfunctions $h(x)$ are either even or odd, if the point $x=0$ is set at the slit center, see Fig. 1(a). One can easily obtain explicit expressions for the eigenfunctions and analyze their properties. Owing to the symmetry, it is sufficient to restrict ourselves to $x\geq 0$.

An arbitrary even eigenfunction $h_+(x)$ is given by

$$h_+ = c\begin{cases}\cos(p_dx) & (x<x_d/2),\\ \cos(p_dx_d/2)e^{ip_m(x-x_d/2)} & (x>x_d/2),\end{cases} \qquad (16)$$

if the eigenvalue β^2 entering parameters $p_{d,m}=(\varepsilon_{d,m}k_0^2 -\beta^2)^{1/2}$ satisfies Eq. (9) with sign (+). It is applicable thus to the propagating and evanescent modes, as well as to the anomalous modes with $p_m''>0$. The constant c can be chosen as convenient. Since the norm squared $\langle h|h\rangle_\varepsilon$ is zero for the anomalous modes, particular choices of c are of little importance.

The following simple observations are useful:

(i) For any anomalous even mode with $p_m''<0$, whose eigenvalue satisfies Eq. (11), one must replace p_m by $-p_m$. This means merely complex conjugation of the function $h_+(x)$ for $p_m''>0$.

(ii) For the odd modes, it is sufficient to replace the cos function in Eq. (16) by the sin function.

(iii) For the propagating and evanescent modes, the eigenfunctions are real.

(iv) For the propagating modes, the values of $p_{d,m}$ are imaginary so that the trigonometric functions transform into real hypergeometric ones.
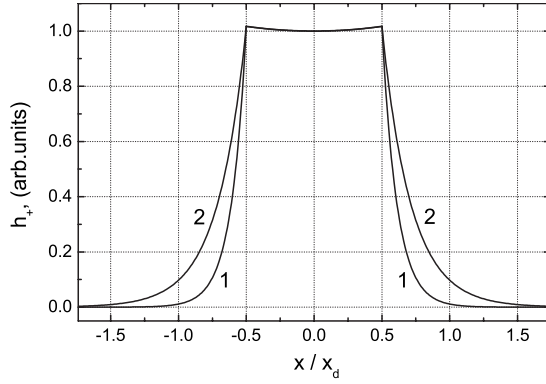
FIG. 5. Spatial profile of the single propagating mode for ε_m $=-10$. Lines 1 and 2 are plotted for $x_d/\lambda=1/4$ and $1/8$.

Figure 5 shows the eigenfunction $h_+(x)$ for the single propagation mode, $\varepsilon_m=-10$, and two subwavelength slits: $x_d/\lambda=1/4$ and $1/8$. The field is practically uniform inside the slit and decreases very rapidly in the metal. The thinner the slit, the smaller is the absolute (not normalized to x_d) decay distance in the metal.

4. Energy flow

Specific properties of different eigenmodes become apparent when we consider the corresponding distributions of the energy flow, i.e., the stream lines of the Pointing vector **P** $=(\mathbf{E}\times\mathbf{H})/4\pi$. Being expressed in terms of the amplitude h, the x and z components of the Pointing vector are

$$P_x = \frac{1}{4\pi}\left(-\frac{i}{\varepsilon}h^*\frac{dh}{dx}+\text{c.c.}\right)\exp(-2\beta''z),$$

$$P_z = \frac{\beta'}{2\pi\varepsilon}|h|^2\exp(-2\beta''z). \qquad (17)$$

The direction of **P** depends on the sign of $\varepsilon(x)$. Inside the slit, where $\varepsilon=\varepsilon_d>0$, we have $P_z\propto\beta'$.

For the propagating modes we have $P_x=0$ and $\beta''=0$ in the lossless case. This means that the Pointing vector $\mathbf{P}(x)$ is parallel and antiparallel to the z axis inside and outside the slit, respectively, for the positive propagation constant β. The total energy flux, $\int P_z(x)dx$, is proportional here to the norm squared $\langle h|h\rangle_\varepsilon$ defined by Eq. (4). One can make sure that this norm is positive, i.e., the energy flow inside the slit is dominating and the positive sign of β leads to a positive total energy flux.

For the evanescent modes, the propagation constant β is purely imaginary in the lossless case. Correspondingly, we have here $P_{x,z}=0$ for the eigenfunctions of the discrete spectrum. Note that $P_x\neq0$ for the evanescent modes of the continuous spectrum, $\beta''/k_0>|\varepsilon_m|$, see also below.

A new situation occurs for the anomalous modes where the propagation constant β is complex for $\varepsilon_m''=0$. Both components of the Pointing vector, P_x and P_z, are nonzero functions of x and z in this case.

Furthermore, we claim that the norm squared $\langle h|h\rangle_\varepsilon$ is zero for the anomalous modes in the lossless case. This im-
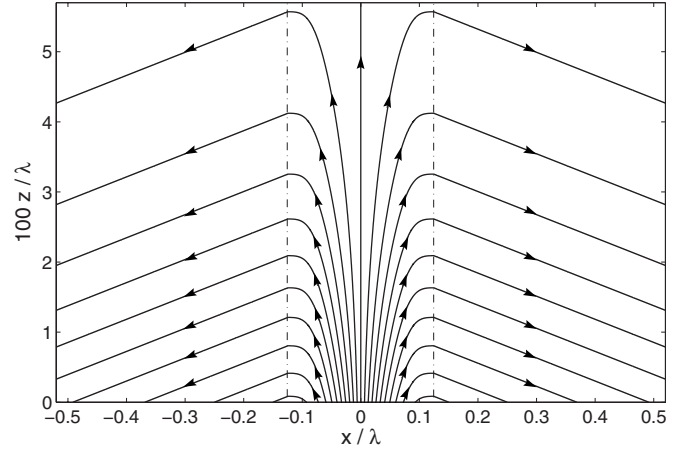
FIG. 6. Streamlines of the Pointing vector for the first anomalous symmetric mode with $\beta'>0$. The dashed vertical lines show the wall positions. Increasing (with z) distance between neighboring lines shows qualitatively decreasing energy flow.

portant property can be proven straightforwardly: An anomalous eigenfunction $h_a(x)$ obeys Eq. (5) with a complex eigenvalue β_a^2. Multiplying the left- and right-hand sides of this equation by $h^*(x)$ and taking the imaginary part of the resulting relation, it is easy to see that the norm squared is proportional to the integral $\int\varepsilon^{-1}\,\text{Im}[h_a^*(d^2h_a/dx^2)]dx$. Integrating it by parts inside and outside the slit and using the continuity of $h_a(x)$ and $\varepsilon^{-1}(x)dh_a/dx$ at the walls, we calculate readily that this integral is zero. It is also not difficult to prove that the norm squared is zero using the explicit expression (16) for the eigenfunction and the corresponding complex eigenvalue β^2.

Looking now at Eqs. (17), we see that the z component of the total energy flux, $\int P_z(x,z)dx$, is zero for any anomalous mode and for any value of the propagation coordinate z. As for the x component of the total energy flux, it is zero by symmetry. All this means is that the forward energy flow in air transforms to the backward flow in metal, and the lateral energy transfer takes place. This is illustrated by Fig. 6 showing the streamlines of the Pointing vector for the first anomalous mode with $\beta'>0$, $\varepsilon_m=-10$, and $x_d/\lambda=1/4$. The x component of the Pointing vector is positive here at the wall $x_d/2$ (the energy outflow). Outside the slit, the streamlines are straight and mutually parallel. The ratio P_z/P_x can be approximated here by $\beta'/\sqrt{\beta''^2-k_0^2|\varepsilon_m|}$. It decreases with increasing β''.

What is the difference between two anomalous modes with $\beta''>0$ and the opposite values of β'? The answer is as follows: One of such modes, namely the mode with $\beta'>0$, corresponds to the outflow of light energy from the slit. The other one (with $\beta'<0$) corresponds to the energy inflow. The conjugate anomalous mode gives an inflow of the light energy into the slit. All arrows in Fig. 6 must be inverted in this case.

Note that the sign of β' does not indicate the propagation direction for the anomalous modes. The positive ($+z$) propagation direction corresponds here to $\beta''>0$, i.e., to decay of the wave amplitude at $z=\infty$.

B. Nonlocalized solutions: Continuous spectrum

The line $\text{Im}(\beta^2)=0$, $\text{Re}(\beta^2)<-|\varepsilon_m|k_0^2$ on the complex β^2 plain, where both parameters $p_{d,m}$ are real quantities and $h(x)$ is not decreasing for $|x|\to\infty$, represents the continuous spectrum of the eigenvalues in the lossless case, see Fig. 2. It is easy to construct directly the evanescent solutions of Eq. (5) for an arbitrary point of this line. For an even eigenfunction we have

$$h_+ = c \begin{cases} \cos(p_d x) & (x < x_d/2), \\ Q\cos(p_m x - \varphi) & (x > x_d/2), \end{cases} \tag{18}$$

where $Q=\cos(p_d x_d/2)/\cos\phi$, $\varphi=\phi+p_m x_d/2$, and $\tan\phi=(p_d/|\varepsilon_m|p_m)\tan(p_d x_d/2)$. Similarly one can represent the odd modes of the continuous spectrum $h_-(x)$. The sin functions in Eq. (18) must be replaced by cos functions to make it so. A double degeneration of the eigenstates of the continuous spectrum thus takes place.

For the above-introduced eigenstates the energy flow is zero, $P_{x,z}=0$. However, for the combinations $h_+\pm ih_-$, which can also serve (owing to the degeneracy) as the basic eigenfunctions, we have $P_x\neq 0$. The eigenfunctions of the continuous spectrum thus provide nonvanishing energy flow to $\pm\infty$. This property is not specific for the slit case; similar modes (known also as nonuniform waves[9]) exist in any slitless metal.

With a weak light absorption taken into account, the straight line $\beta''/k_0>\sqrt{|\varepsilon_m'|}$, $\beta'/k_0=0$, representing the continuous spectrum, transforms to the line $\beta'\beta''/k_0^2=\varepsilon_m''/2$, $\beta''/k_0\gtrsim\sqrt{|\varepsilon_m'|}$, i.e., slightly bends and shifts to the right, see Fig. 2(a).

IV. ONE-DIMENSIONAL PHOTONIC CRYSTAL

Our second particular structure is 1D photonic crystal depicted in Fig. 1(b). The slit and wall widths are x_d and x_m, respectively, the period is $x_0=x_d+x_m$, and the permittivities $\varepsilon_{d,m}$ are generally complex.

Solution of Eq. (1) for an eigenmode now has the form

$$H(x) = e^{i\kappa x + i\beta z}h(x), \tag{19}$$

where κ is the Bloch wave vector ranging from $-\pi/x_0$ to π/x_0 and $h(x)$ is an x_0 periodic function. Within each of the regions, slit (d) and metal (m), it is a linear combination of two exponential functions,

$$h_{d,m}(x) = c_{d,m}^+ e^{i(p_{d,m}-\kappa)x} + c_{d,m}^- e^{-i(p_{d,m}+\kappa)x}, \tag{20}$$

where $c_{d,m}^\pm$ are four constants and $p_{d,m}$ are given again by Eq. (6).

A. Eigenvalues

Using continuity of $H(x)$ and $E_z(x)\propto\varepsilon^{-1}dH/dx$ at the interfaces (i.e., the true boundary conditions) and the periodicity of $h(x)$ and dh/dx, we come to a set of four linear algebraic equations for the constants $c_{d,m}^\pm$. The condition of solvability of this set (the zero determinant condition) gives a new dispersion equation for the eigenvalue β^2. After routine calculations, this equation can be presented in the form:

$$\frac{1}{2}\left(\frac{p_d\varepsilon_m}{p_m\varepsilon_d} + \frac{p_m\varepsilon_d}{p_d\varepsilon_m}\right)\sin(p_d x_d)\sin(p_m x_m)$$
$$= \cos(p_d x_d)\cos(p_m x_m) - \cos(\kappa x_0). \tag{21}$$

It generalizes Eq. (13) of Ref. 12 in the sense that the permittivity in the slit regions, ε_d, can be different from 1. The trigonometric functions possess generally complex arguments. If $\varepsilon_{d,m}$ are real, Eq. (21) for $\xi=\beta^2/k_0^2$ is real as well.

One can check that the following scaling relation for β takes place:

$$\beta(k_0 x_d, k_0 x_m, \varepsilon_m, \varepsilon_d, \kappa x_0)$$
$$= \sqrt{\varepsilon_d}\beta(\sqrt{\varepsilon_d}k_0 x_d, \sqrt{\varepsilon_d}k_0 x_m, \varepsilon_m/\varepsilon_d, 1, \kappa x_0). \tag{22}$$

It is similar to Eq. (12) for the single slit and allows us again to restrict ourselves to the case $\varepsilon_d=1$ (air slits).

For practical purposes, the ratios λ/x_0 and x_m/x_d are sometimes more useful for analysis of the eigenmodes than the products $k_0 x_d$ and $k_0 x_m$.

1. The case $\kappa=0$

Often, the Bloch wave vector κ equals the transverse component of the wave vector of a plane wave which is incident onto the photonic crystal. In the case of normal incidence, which is of prime importance for the ELT and is also the simplest in symmetry, we are at the center of the Brillouin zone, $\kappa=0$. This is why we pay special attention to this particular case.

For $\kappa=0$, each eigenmode is either even or odd, $h(x)=\pm h(-x)$, if we set the point $x=0$ at the slit center, see Fig. 1(b). The dispersion equation (21) can be split here into two separate equations:

$$\frac{p_{d,m}}{\varepsilon_{d,m}}\tan\left(\frac{p_d x_d}{2}\right) + \frac{p_{m,d}}{\varepsilon_{m,d}}\tan\left(\frac{p_m x_m}{2}\right) = 0. \tag{23}$$

The first and second of the double subscripts correspond to the even and odd modes, respectively. The values of β^2 for these modes are different.

Each of Eqs. (23) gives a sequence of real roots, positive and negative, for β^2/k_0^2 in the lossless case. These roots correspond to the propagating and evanescent modes. In the dielectric case, $\varepsilon_{d,m}'>0$, this sequence is complete—there are no longer any solutions for β^2/k_0^2. However, in the metal-dielectric case, $\varepsilon_d'>0$, $\varepsilon_m'<0$, there is again an additional sequence of complex mutually conjugate roots for β^2/k_0^2 which corresponds to the anomalous modes.

The circles in Fig. 7(a) show the values of the propagation constant $\beta=+\sqrt{\beta^2}$ for $\kappa=0$, $x_d=x_0/5=\lambda/4$, $\varepsilon_d=1$, and $\varepsilon_m=-10$. Like in Fig. 2(a), we have a single even propagating mode with $\beta/k_0\approx 1.2$, a single odd evanescent mode with $\beta/k_0\approx 1.6i$, and a sequence of even and odd anomalous modes with $\beta''/k_0>\sqrt{|\varepsilon_m|}$ and $\beta'\neq 0$. One of the differences between the periodic case in question and the single-slit case is the presence of a discrete sequence of the evanescent roots with $\beta''/k_0>\sqrt{|\varepsilon_m|}$ and $\beta'=0$ instead of the continuous spectrum. About 30% of the modes in Fig. 7(a) are anomalous.

With weak losses taken into account, the roots experience small displacements. The strongest of them (slight shifts to
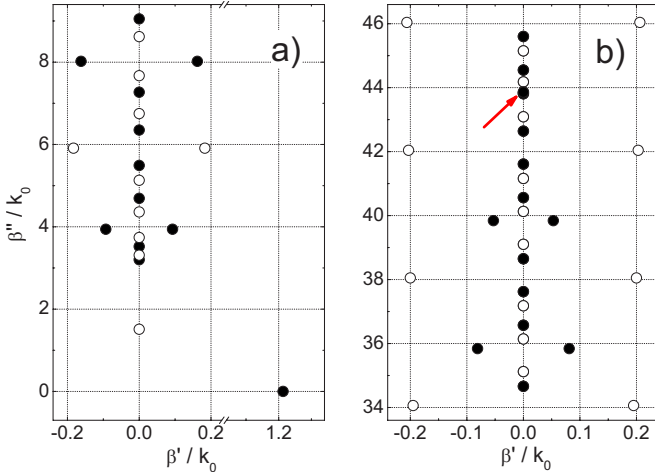
FIG. 7. (Color online) Values of β/k_0 for a periodic structure with $\varepsilon_m = -10$ and $x_m = 4x_d = \lambda$. The filled and open circles correspond to the even and odd modes at $\varepsilon_m'' = 0$. Case (b) refers to large values of β''/k_0. The arrow indicates two closely situated evanescent roots originating from the confluence of a pair of "even" anomalous roots.

FIG. 8. The ratios β'/k_0 and β''/k_0 versus λ/x_d for $\varepsilon_m = -10$ and $\lambda/x_m = 1$. The black and gray lines correspond to the evanescent and anomalous roots, respectively.

the right) occur for the evanescent roots. The other displacements do not exceed the circle size.

In many respects, the changes in the spectrum of β with changing parameters x_d and ε_m are similar to the above described changes for the single-slit case. With decreasing slit width x_d, the propagating mode survives (β' grows as x_d^{-1}), the evanescent mode with $\beta''/k_0 < \sqrt{|\varepsilon_m|}$ disappears, and the vertical separation between the anomalous roots increases as $2\pi/x_d$. With increasing x_d, the number of propagating modes and the number of evanescent modes with $\beta''/k_0 < \sqrt{|\varepsilon_m|}$ increase. With increasing $|\varepsilon_m|$, the value of β/k_0 for the propagating mode decreases, the density of the anomalous roots decreases as well, and still one evanescent root with $\beta''/k_0 < |\varepsilon_m|^{1/2}$ is present.

Increasing wall thickness x_m does not strongly affect the propagating and anomalous roots in Fig. 7(a). However, the density of the evanescent modes in the region $\beta''/k_0 > \sqrt{|\varepsilon_m|}$ increases $\propto x_m$. In the limit $x_m \to \infty$ we come to the continuous spectrum of the single-slit case.

Despite the mentioned similarities with the single-slit case, there are important differences. To highlight them, we recall that our periodic 1D structure can be characterized by the effective dielectric permittivity ε_{eff} in the long-wave limit, $\lambda/2\pi|\varepsilon_m| \gg x_m$, when the metal walls become skin thin.[29] This permittivity is expressed by the average over the period, $\varepsilon_{\text{eff}} = \langle \varepsilon^{-1}(x) \rangle^{-1} = |\varepsilon_m| x_0/(|\varepsilon_m| x_d - x_m)$. It is positive for $x_m/x_d < |\varepsilon_m|$, negative for $x_m/x_d > |\varepsilon_m|$, and infinite at $x_m/x_d = |\varepsilon_m|$. It turns out that the properties of the anomalous modes are essentially different in the above two regions of $x_m/x_d|\varepsilon_m|$ even when we are far from the long-wave limit.

Our analysis shows that for $\varepsilon_m < -1$ the total number of even anomalous modes is infinite only for $x_m/x_d > |\varepsilon_m|$ when $\varepsilon_{\text{eff}} < 0$, i.e., for sufficiently large wall widths. How big is this number in the case $x_m/x_d < |\varepsilon_m|$? The number of even modes grows with decreasing λ/x_0 and increasing ε_{eff}. For example, in the case of Fig. 7 (where $\varepsilon_m = -10$, $x_m/x_d = 4$, and
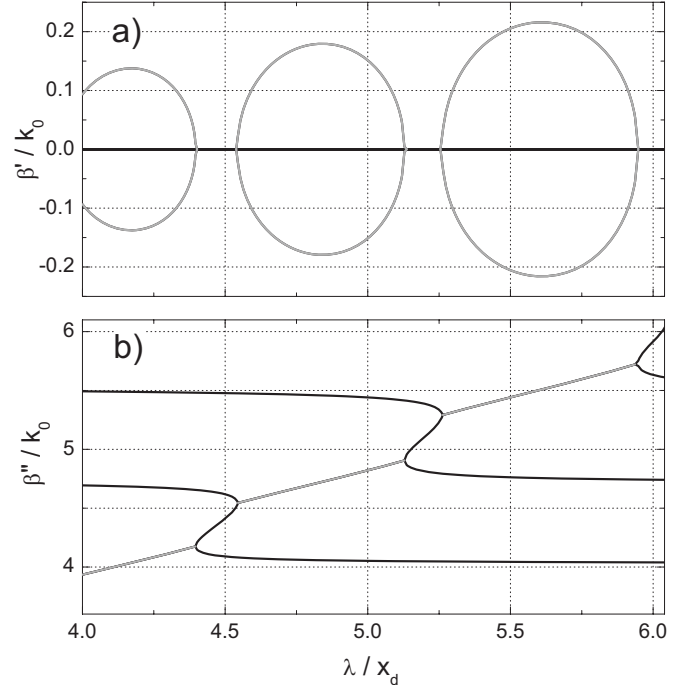
$\lambda/x_0 = 0.8$) there are 10 pair of even roots and for the last pair $\beta''/k_0 \simeq 39.8$. Switching ε_m to -6 increases the number of pairs to 18. Disappearance of the "even" anomalous roots with increasing β''/k_0 occurs via decreasing horizontal separation $2|\beta'|$ and transformation into a pair of purely imaginary evanescent roots, see Fig. 7(b). The number of odd anomalous modes remains infinite for $\varepsilon_m < -1$. Persistence of the these modes in the range of large β''/k_0 is also illustrated by Fig. 7(b).

For $-1 < \varepsilon_m < 0$, the situation is inverse: The number of even anomalous modes is always infinite while the number of odd modes is finite only for $x_m/x_d < |\varepsilon_m|$.

The conclusion about the relationship between ε_{eff} and the total number of anomalous roots is based not only on numerical calculations but also on our analytical studies of the special case $x_m/x_d = 4$. It admits a complete analytical analysis in the long-wave limit.

One more difference of the periodic case from the single-slit case is mutual transformations between the discrete anomalous and evanescent roots of the same parity when changing parameters $k_0 x_{d,m}$ and ε_m. This is illustrated by Fig. 8 that shows the dependences of β'/k_0 and β''/k_0 on the ratio λ/x_d for $\lambda/x_m = 1$, $\varepsilon_m = -10$, and the even modes with $\beta''/k_0 < 6$. At $\lambda/x_d = 4$ we have, in accordance with Fig. 7(a), a pair of anomalous roots with $\beta/k_0 \simeq \pm 0.1 + 3.9i$ and two higher-lying evanescent roots $\beta/k_0 \simeq 4.7i$ and $5.5i$. When λ/x_d increases, the value of β''/k_0 for the anomalous roots grows relatively quickly and approaches the nearest evanescent root. At the same time, the horizontal separation $2|\beta'/k_0|$ first increases and then tends quickly to zero. At $\lambda/x_d \simeq 4.4$ the anomalous roots confluence and transform into a pair of new evanescent roots with rapidly increasing vertical sepa-
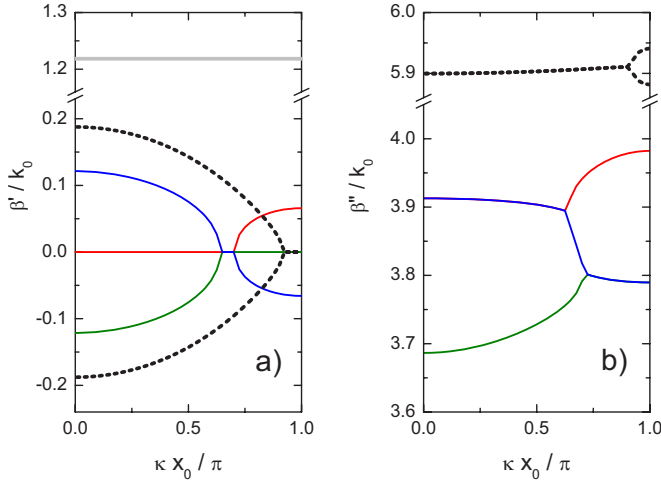
FIG. 9. (Color online) Dependences $\beta'(\kappa)$ and $\beta''(\kappa)$ for the periodic structure with $x_0=5x_d=5\lambda/4$, and $\varepsilon_m=-9.6$. Solid lines are plotted for the first pair of anomalous modes and the nearest evanescent mode, the dotted lines correspond to the second anomalous pair, and the gray line is for the propagating mode.

ration. The largest of these roots grows quickly with further increasing λ/x_d and confluences with the nearest evanescent root giving rise to a new pair of the anomalous roots. This occurs at $\lambda/x_d\simeq4.54$. Then the processes of mutual transformation continue. The same scenario holds for the other even roots and also for the odd roots; the transformations for the latter occur at different values of λ/x_d.

Three general features of the transformations are worthy of mentioning:

(i) Only approaching anomalous roots trigger the changes of β''/k_0 for the evanescent roots.

(ii) The transformations occur in a critical manner, i.e., according to the square-root law in the close vicinity of the threshold.

(iii) The roots cannot appear or disappear when varying characteristic parameters. Only quantitative changes and transformations between pairs of anomalous and evanescent roots of the same parity take place.

2. Peculiarities of Bloch diagrams

Consider now dependences of the eigenvalues on the Bloch wave vector κ. They are important for analysis of the transmission and reflection properties in the case of tilted incidence of a plane wave onto the photonic crystal. The Bloch dependences $\beta'(\kappa)$ and $\beta''(\kappa)$ for the propagating and evanescent modes, which are solely present in the literature, are insufficient in the metal-dielectric case where the anomalous modes are present. Moreover, the anomalous modes cause interaction of different branches and strong peculiarities of the Bloch diagrams.

For $\kappa\neq0$ the eigenmodes cannot be separated in even and odd and the general dispersion equation (21) must be used. Each value of β calculated for $\kappa=0$ initiates a branch $\beta(\kappa)$. Figure 9 shows examples of the κ dependences for our 1D periodic structure. The value of $|\beta'|$ for the first pair of anomalous modes [see Fig. 7(a)] decreases with growing κ

and turns to zero for $0.66\lesssim\kappa x_0/\pi\lesssim0.71$, i.e., the anomalous modes become evanescent within this interval. For $\kappa x_0/\pi\gtrsim0.71$ a pair of anomalous modes appears again. This behavior is correlated with bifurcations of $\beta''(\kappa)$ for the anomalous modes and the nearest evanescent mode. Behavior of the second pair of anomalous modes is different. The confluence of the branches $\beta'(\kappa)$ for these modes at $\kappa x_0/\pi\simeq0.9$ is accompanied by the split of $\beta''(\kappa)$. The dependence $\beta(\kappa)$ for the propagating mode and most of the evanescent modes is fairly weak.

Only neighboring anomalous and evanescent roots affect each other. In this sense, the bifurcations in the above κ dependences are similar to those in the λ/x_d dependences presented in Fig. 8.

B. Eigenfunctions

Construction of the eigenfunctions in the periodic case for $\kappa=0$ is similar to that in the single-slit case, see Eq. (16). In particular, setting the point $x=0$ at the slit center we have for an even eigenfunction inside and outside the slit,

$$h_+ = c\begin{cases}\cos(0.5p_mx_m)\cos(p_dx) & \text{(in)}\\ \cos(0.5p_dx_d)\cos[p_m(x-0.5x_0)] & \text{(out)}.\end{cases} \quad (24)$$

It is applicable to the propagating, evanescent, and anomalous modes. One can check that $h_+(x)$ is even also with respect to the wall center. Similarly, one can construct the odd eigenfunctions. Using the dispersion relation (23) for the even modes, one can show explicitly the validity of the orthogonality relations. The integration in x must be performed over the period x_0.

Our analysis of the light energy flows for different modes, made earlier for the single-slit case, is fully applicable to the periodic case in question, if we restrict our considerations to the period x_0.

V. SINGLE CIRCULAR HOLE

The last waveguiding structure to consider is a circular hole, see Fig. 1(c). Inside and outside the hole ($r<R$ and $r>R$) each of the field components E_z, H_z can be set proportional to $I_j(s_dr)\exp(ij\varphi+i\beta z)$ and $K_j(s_mr)\exp(ij\varphi+i\beta z)$, respectively. Here $r=\sqrt{x^2+y^2}$ is the radial coordinate, φ is the azimuth angle, $j=0,\pm1,\pm2,\dots$ is the azimuth number, I_j and K_j are the modified Bessel and MacDonald functions of order j,[27] and $s_{d,m}=ip_{d,m}=(\beta^2-\varepsilon_{d,m}k_0^2)^{1/2}$. The quantities $s_{d,m}$ are generally complex. The other field components in the cylindrical coordinate system, E_r, E_φ, H_r, and H_φ, can be expressed by E_z and H_z using Maxwell's equations. All field components are expected to be zero for $r\to\infty$.

Using the boundary conditions for the field components at $r=R$, we come to the known dispersion equation for β^2,[10,30,31]

$$\left(\frac{\varepsilon_dI_j'}{s_dI_j}-\frac{\varepsilon_mK_j'}{s_mK_j}\right)\left(\frac{I_j'}{s_dI_j}-\frac{K_j'}{s_mK_j}\right)=\frac{j^2\beta^2}{k_0^2R^2}\left(\frac{1}{s_d^2}-\frac{1}{s_m^2}\right)^2, \quad (25)$$

where the prime means taking the derivative with respect to the argument and the arguments of the functions I_j and K_j are
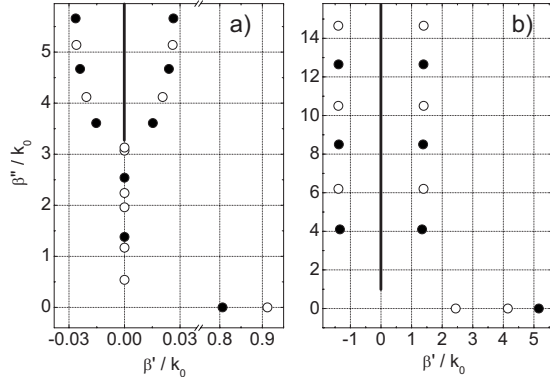
FIG. 10. The values of the propagation constant β for the circular hole and $j=0,1$. Case (a) corresponds to $R=\lambda/2$ and $\varepsilon_m=-10$; for the case (b) $R=\lambda/8$ and $\varepsilon_m=-0.8$. The filled and open circles correspond to $j=0$ and 1, respectively. The vertical solid lines show the continuous spectrum.

$s_d R$ and $s_m R$, respectively; they are generally complex. Note that Eq. (25) can be rewritten in an equivalent form via the Bessel functions and the first-kind Hankel functions. Furthermore, using the recursion relations for the Bessel functions,[27] one can get rid of the derivatives in Eq. (25).

Solutions for β/k_0 are determined by three dimensionless parameters, $k_0 R$, ε_d, and ε_m. One can check that the scaling relation $\beta(k_0 R, \varepsilon_m, \varepsilon_d) = \sqrt{\varepsilon_d} \beta(\sqrt{\varepsilon_d} k_0 R, \varepsilon_m/\varepsilon_d, 1)$ is applicable; it is similar to Eq. (12) for the single-slit case. It is sufficient thus to consider, as earlier, the case $\varepsilon_d=1$.

At $j=0$ the dispersion equation splits into two separate equations. One of them [equality to zero of the first large parentheses in Eq. (25)] is for the TM modes, $H_z=0$, while the other (equality to zero of the second large parentheses) is for the TE modes, $E_z=0$. For $j \neq 0$, the modes are hybrid—both E_z and H_z are nonzero.

Figure 10 shows two representative examples of the spectrum of β for the azimuth number $j=0$ and 1. The case (a) is $\varepsilon_m=-10$ and $R=\lambda/2$, this radius is slightly above its critical value for the ideal metal, $\simeq 0.3\lambda$. We have two propagating modes, the largest value of β corresponds to $j=1$ (to the HE_{11} mode). Additionally, we have several evanescent modes (two of them, with $\beta \simeq 3i$, are due to transform into a pair of anomalous modes), a sequence of anomalous modes with pretty small horizontal separations, and a continuous spectrum $\beta'=0$, $\beta''/k_0 > \sqrt{|\varepsilon_m|}$. In general, the situation is similar to that for the single-slit case, compare with Fig. 2. With decreasing R, the propagating roots move toward zero and transform here into evanescent roots, i.e., the modal cutoff takes place in contrast to the slit case. This distinction is not surprising; it is caused by the geometric and polarization differences between the 1D and 2D eigenfunctions. The evanescent roots, in turn, move toward $i\sqrt{|\varepsilon_m|}$ with decreasing R and transform into anomalous roots; scenario of this transformation is qualitatively the same as it is in the single-slit case.

Case (b) corresponds to $-1<\varepsilon_m$ and an ultranarrow hole, $R=\lambda/8$. We have here three propagating modes and the largest value of β corresponds to the TM mode $(j=0)$. The evanescent modes are absent. The other features—localized
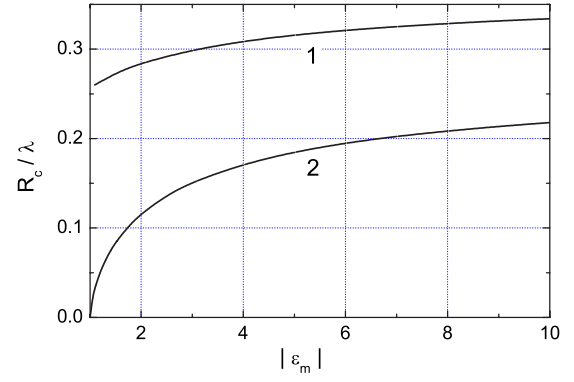
FIG. 11. (Color online) Critical radius R_c versus $(|\varepsilon_m|)$ for the azimuth numbers $j=0$ (line 1) and 1 (line 2).

anomalous modes with relatively large horizontal separations and a continuous spectrum—are well recognizable. The propagating roots with $|j|>1$ are absent. Furthermore, the shown propagating roots *do not* disappear with decreasing R. This feature is rather surprising and promising for the extraordinary transmission phenomena.

The presented data raise an important question: What is the minimum possible hole radius R for the propagating modes? The rest of this section is devoted to answer this question.

For $|\varepsilon_m|>1$, the propagating modes exist only for sufficiently large values of the radius, $R>R_c$, where the critical radius R_c depends on $|\varepsilon_m|$ and also on j^2. At $R=R_c$, the eigenvalue β^2 changes its sign, i.e., the propagating mode transforms into an evanescent one. Figure 11 shows the dependence $R_c(\varepsilon_m)$ for $m=0$ and 1; the values of R_c for $j^2>1$ lie considerably higher. The lowest branch corresponds to $|j|=1$. With ε_m approaching -1 the value of R_c tends to zero.

The situation with the propagating modes in the range $-1<\varepsilon_m<0$ is entirely different. At least one propagating mode exists here for *arbitrary small* radius R. In the limit $k_0 R \ll 1$, $\beta/k_0 \gg 1$, the right-hand side of Eq. (25) is negligible, $s_{d,m} \simeq \beta$, and the dispersion equation simplifies to $|\varepsilon_m|=F_j(\beta R)$, where $F_j=-(K_j I_j')/(I_j K_j')$. Figure 12 shows the dependence $F_j(\beta R)$ for $j=0$, 1, and 2. One sees that the lowest branch $F_0(\beta R)$ grows monotonically from 0 to 1,
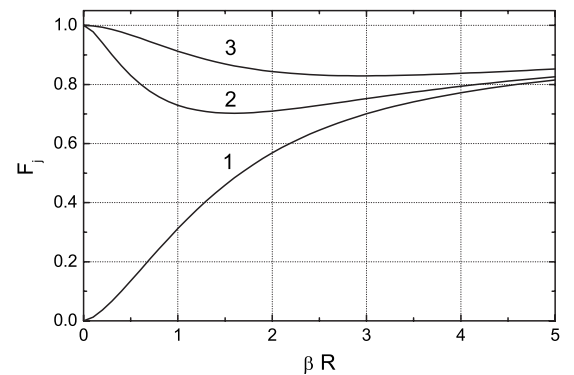
FIG. 12. Dependence $F_j(\beta R)$ for the propagating modes in the case $0>\varepsilon_m>-1$, $k_0 R \ll 1$. Curves 1, 2, and 3 correspond to the azimuth number $j=0$, 1, and 2, respectively.

whereas the higher branches decrease first from 1 to certain minimum values and grow then very slowly approaching unity.

As follows from this analysis, we always have a single propagating mode with $j=0$; the corresponding value of the propagating constant is given by $\beta_0 = R^{-1} F_0^{-1}(|\varepsilon_m|)$. For the branch with $j=1$, equation $F_1(\beta R) = |\varepsilon_m|$ has two solutions for $1 > |\varepsilon_m| > 0.71$ and no solutions outside the indicated interval of $|\varepsilon|$. When the azimuth number $|j|$ is increasing, the allowed interval of $|\varepsilon_m|$ is shrinking. For $0 < 1 + \varepsilon_m \ll 1$ there is a waste variety of the propagating modes with $R \ll \lambda$.

Note that the condition $\varepsilon_m/\varepsilon_d > -1$, which is sufficient to realize the propagating modes for ultranarrow holes, can be achieved with many real metals using the dielectric component with sufficiently high value of the refractive index $\sqrt{\varepsilon_d}$.

Our results on the presence of the propagating modes in ultranarrow circular holes are in line with the recent conclusions of Ref. 32. In contrast to this paper, we did not use, however, model assumptions concerning the frequency dependence of ε_m. Our approach relies solely on the concept of the dielectric permittivity.

VI. SUMMARY

The eigenmode problem for metal-dielectric structures, photonic crystals, single slits, and holes in metal, is essentially different from that typical of dielectric structures and quantum mechanics. It is not Hermitian and the eigenvalues are generally complex in the lossless case.

In addition to the propagating and evanescent modes, there is a sequence of pairs of anomalous eigenmodes with complex conjugate eigenvalues. For single slits and holes, these modes are fully localized—the corresponding eigenfunctions tend to zero at infinity.

The anomalous eigenmodes provide a lateral transfer of the light energy between the dielectric and metal counterparts. The total energy flow is zero in the lossless case.

For periodic 1D structures, the number of anomalous modes is determined by the ratio $x_m \varepsilon_d/x_d |\varepsilon_m|$. For $x_m/x_d > |\varepsilon_m|/\varepsilon_d$, which corresponds to the effective long-wave permittivity $\varepsilon_{\text{eff}} < 0$, the number of even anomalous modes is infinite. In the opposite case, the sequence of the even anomalous modes is finite.

The presence of anomalous modes causes strong peculiarities of the Bloch diagrams for periodic 1D structures.

Solutions for the propagating constant β obey scaling relations. They allow to extend the conditions for existence of the propagating modes by filling the slits and/or holes with transparent dielectrics.

Whereas at least one propagating mode always exists in 1D slits, in circular 2D holes the cutoff for the propagating modes is absent only for $0 > \varepsilon_m/\varepsilon_d > -1$.

The results obtained form an infrastructure for modelling of the extraordinary light transmission phenomenon.

[1] A. Yariv and P. Yeh, *Optical Waves in Crystals* (Wiley, New York, 2003), Chap. 11.

[2] C. Vassalo, *Optical Waveguide Concepts* (Elsevier, New York, 1991).

[3] A. W. Snyder and J. D. Love, *Theory of Optical Waveguides* (Chapman and Hall, New York, 1983).

[4] H. Kogelnik, "Theory of optical waveguides," in *Guided-wave Optoelectronics*, edited by T. Tamir (Springer-Verlag, Berlin, 1990).

[5] R. E. Collin, *Field Theory of Guided Waves* (Wiley, New York, 1991).

[6] J. D. Joannopoulos, R. D. Meade, and J. N. Winn, *Photonic Crystals* (Princeton University Press, Princeton, NJ, 1995).

[7] K. Sakoda, *Optical Properties of Photonic Crystals* (Springer-Verlag, Berlin, 2001).

[8] I. P. Kaminov, W. L. Mammel, and H. P. Weber, Appl. Opt. **13**, 396 (1974).

[9] L. D. Landau and E. M. Lifshitz, *Electrodynamics of Continuous Media* (Pergamon, New York, 2004).

[10] J. D. Jackson, *Classical Electrodynamics* (Wiley, New York, 1975).

[11] B. Prade and J. Y. Vinet, J. Lightwave Technol. **12**, 6 (1994).

[12] P. Sheng, R. S. Stepleman, and P. N. Sanda, Phys. Rev. B **26**, 2907 (1982).

[13] D. M. Whittaker and I. S. Culshaw, Phys. Rev. B **60**, 2610 (1999).

[14] H. Raether, *Surface Plasmons* (Springer-Verlag, Berlin, 1998).

[15] W. L. Barnes, A. Dereux, and T. W. Ebbesen, Nature (London) **424**, 824 (2003).

[16] P. B. Jonson and R. W. Christy, Phys. Rev. B **6**, 4370 (1972).

[17] T. W. Ebbesen, H. J. Lezec, H. F. Ghaemi, T. Thio, and P. A. Wolff, Nature (London) **391**, 667 (1998).

[18] J. A. Porto, F. J. Garcia-Vidal, and J. B. Pendry, Phys. Rev. Lett. **83**, 2845 (1999); F. J. Garcia-Vidal and L. Martin-Moreno, Phys. Rev. B **66**, 155412 (2002).

[19] M. M. J. Treacy, Phys. Rev. B **66**, 195105 (2002).

[20] P. Lalanne, J. P. Hugonin, and J. C. Rodier, Phys. Rev. Lett. **95**, 263902 (2005).

[21] P. N. Stavrinou and L. Solymar, Opt. Commun. **206**, 217 (2002).

[22] Y. Xie, A. R. Zakharian, J. V. Moloney, and M. Mansuripur, Opt. Express **14**, 6400 (2006).

[23] S. G. Tikhodeev, A. L. Yablonskii, E. A. Muljarov, N. A. Gippius, and T. Ishihara, Phys. Rev. B **66**, 045102 (2002).

[24] J. Mathews and R. L. Walker, *Mathematical Methods of Physics* (W. A. Benjamin, New York, 1964), Chap. 6.

[25] B. Sturman, E. Podivilov, and M. Gorkunov, Europhys. Lett., (to be published); arXiv:cond-mat/0609753.

[26] C. Kittel, *Quantum Theory of Solids* (Wiley, New York, 1987).

[27] H. Bateman and A. Erdelyi, *Higher Transcendental Functions* (McGraw-Hill, New York, 1953), Vol. 2.

[28] *Handbook of Optics*, edited by M. Bass (McGraw-Hill, New York, 1995), Vol. 2.

[29] A. Yariv and P. Yeh, J. Opt. Soc. Am. **67**, 423 (1977).

[30] C. A. Pfeiffer, E. N. Economou, and K. L. Ngai, Phys. Rev. B **10**, 3038 (1974).

[31] L. Novotny and C. Hafner, Phys. Rev. E **50**, 4094 (1994).

[32] P. B. Catrysse, H. Shin, and S. Fun, J. Vac. Sci. Technol. B **23**, 2675 (2005).